

Network Performance Analysis of Satellite–Terrestrial Vehicular Network

Huaqing Wu¹, *Member, IEEE*, Mingcheng He², *Graduate Student Member, IEEE*,
 Xuemin Shen¹, *Fellow, IEEE*, Weihua Zhuang², *Fellow, IEEE*, Ngọc-Dũng Đào³,
 and Weisen Shi³, *Member, IEEE*

Abstract—The low Earth orbit (LEO) satellite-assisted communications are envisioned as a prospective solution in next-generation networks to provide reliable, flexible, cost-effective, and globally seamless services. In this article, we investigate satellite-terrestrial vehicular network (STVN) supporting connected autonomous vehicle (CAV) applications anytime and anywhere. We first establish a model for the LEO satellite-CAV communication system with different satellite orbital parameters. Then, the LEO satellite-CAV communication performance in terms of service availability, outage probability, and system throughput is analyzed when considering practical satellite constellations. Furthermore, the impact of different terrestrial infrastructure deployment strategies on the STVN performance is investigated. Extensive numerical results are provided to validate our theoretical analysis and demonstrate the improvement of CAV network performance thanks to LEO satellites in the STVN.

Index Terms—Connected autonomous vehicles (CAVs), low Earth orbit (LEO) satellites, satellite-terrestrial vehicular network (STVN).

I. INTRODUCTION

CONNECTED autonomous vehicles (CAVs) are expected to revolutionize the transportation system to improve road safety, transportation efficiency, and driving experiences [1], [2], [3]. With vehicle-to-everything (V2X) communications, ubiquitous information exchanges are enabled to support multifarious CAV applications, including safety-related applications (e.g., collision avoidance), traffic efficiency-related applications (e.g., route planning), and infotainment applications (e.g., video streaming). To empower CAV services, especially in the future driverless era, high data rate and ubiquitous network accessibility are expected. However, since the deployment of terrestrial roadside units

(RSUs) is limited due to high deployment/maintenance cost or geometrical constraints, relying solely on terrestrial networks may hardly guarantee globally flexible and reliable network connectivity [4].

Recently, low Earth orbit (LEO) satellite-assisted communication networks have attracted substantial attention in academia [5], [6] and industry [7], [8], where satellites can provide services to CAVs through service links and couple to ground stations through feeder links. The global availability of LEO satellite networks holds significant potential for enabling worldwide seamless high-bandwidth network connections for CAVs in a cost-effective manner. Furthermore, since LEO satellite networks have large coverage areas and can connect to ground stations in different regions, they are less vulnerable to natural disasters that affect regional terrestrial network services, and thus can provide ultrareliable and robust network connections. However, LEO satellite networks have nonnegligible propagation delay and highly dynamic network topology. In other words, terrestrial and satellite networks have their pros and cons in providing services, such as in terms of coverage, transmission delay, throughput, and reliability. Via effective Internetworking, the complementary advantages of terrestrial and satellite network segments can be leveraged to enhance CAV service qualities. Therefore, it is crucial to investigate the satellite-terrestrial vehicular network (STVN) for CAVs, to provide flexible network management and satisfy diverse requirements for different applications.

A. Related Works

Standardization Activities on Satellite-Terrestrial Network Integration: Standards for satellite-terrestrial network integration have been developed to provide guidance for implementation. The 3rd Generation Partnership Project (3GPP) has undertaken significant standardization efforts in this area. Specifically, standards [9], [10] have been developed to define scenarios and identify service requirements for a new architecture where satellite networks act as an extension to terrestrial networks. In [11] and [12], the new radio (NR) is studied to support nonterrestrial networks (NTN), considering the architecture principles and channel model differences between satellite networks and terrestrial cellular networks. In [13], service application scenarios are divided into three categories when integrating satellite access networks into 5G systems: 1) continuity; 2) ubiquity; and 3) scalability. These 3GPP standards underscore the vital role of satellite

Manuscript received 4 October 2023; revised 21 November 2023 and 22 January 2024; accepted 3 February 2024. Date of publication 16 February 2024; date of current version 25 April 2024. (Corresponding author: Huaqing Wu.)

Huaqing Wu is with the Department of Electrical and Software Engineering, University of Calgary, Calgary, AB T2N 1N4, Canada (e-mail: huaqing.wu1@ucalgary.ca).

Mingcheng He, Xuemin Shen, and Weihua Zhuang are with the Department of Electrical and Computer Engineering, University of Waterloo, Waterloo, ON N2L 3G1, Canada (e-mail: mingcheng.he@uwaterloo.ca; sshen@uwaterloo.ca; wzhuang@uwaterloo.ca).

Ngọc-Dũng Đào and Weisen Shi are with the Ottawa Advanced Wireless Technology Lab, Huawei Canada Research Centre, Ottawa, ON K2K 3J1, Canada (e-mail: ngoc.dao@huawei.com; weisen.shi1@huawei.com).

Digital Object Identifier 10.1109/JIOT.2024.3366873

networks in 5G and beyond communication systems to provide ubiquitous access capability and ensure service quality.

Moreover, the European Telecommunications Standards Institute (ETSI) has put forth standards related to the integration of satellite and terrestrial networks. The definition and classification of scenarios that involve this integration are presented in [14]. The role of satellite networks in disaster management and resource requirements for applications, such as Earth observation, satellite navigation, and satellite communications is identified [15]. The traffic distribution in wireless access networks and a typical scenario of satellite-terrestrial network integration are studied in [16], with satellite backhauling in rural areas.

Satellite Network Performance Analysis: Considering the advantages from LEO satellites, there are many works to analyze network performance in satellite communication. In [17], the outage probability is derived for a downlink LEO satellite communication system with multiple LEO satellites uniformly distributed over a sphere following a homogeneous binomial point process (BPP). This article also addresses the problem of maximizing system throughput through an iterative algorithm. In [18], a relay selection scheme is proposed to enhance the quality of the downlink satellite-terrestrial transmission, based on which the analytical expressions for the outage probability and throughput of the system are derived. In [19], the meta distribution of signal-to-interference-plus-noise ratio (SINR) for the downlink integrated LEO satellite-terrestrial millimeter-wave decode-and-forward relay network is investigated. Taking the satellite movement into account, a nonstationary satellite communication system is modeled in [20]. Considering the variations of the distance between satellites and ground users, the instantaneous outage probability, channel capacity, and system throughput are calculated. In [21], the outage probability is analyzed for an overlay satellite-terrestrial network, where an opportunistically selected terrestrial Internet of Things network assists the primary satellite communications in the presence of hybrid interference from both extra-terrestrial sources and terrestrial sources. In [22], the impact of typical satellite channel characteristics, i.e., large path losses, delays, and Doppler shifts, on the physical and medium access control layers are discussed and assessed.

STVN Architecture Design: In addition to the satellite network performance, researchers have presented results and insights on the satellite-terrestrial integrated network architectures and have raised some open questions in their works. Kota et al. [23] provided detailed definitions and examples of satellite-terrestrial integrated/hybrid networks, and consider related issues in the physical layer, link layer, and network layer. In [24], a space-air-ground integrated vehicular network (SAGVN) is proposed to support vehicular applications with a software-defined networking (SDN) architecture. In [25], an SDN-based hybrid and hierarchical SAGVN control architecture is proposed for flexible, reliable, and scalable CAV service provisioning. AI-based solutions are also investigated to facilitate efficient network management and boost CAV service performance. In [26], an SAGVN architecture is investigated with multidimensional and multiscale context-information and network resources from different network segments.

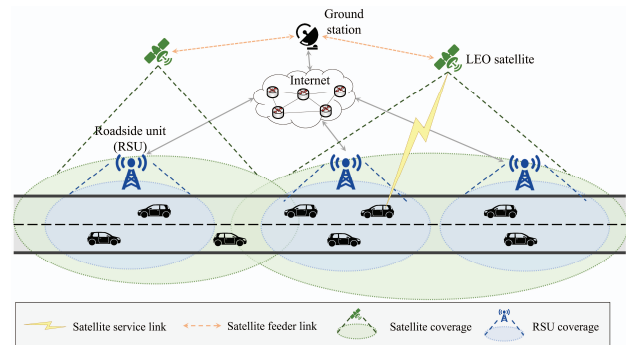


Fig. 1. Illustration of satellite and RSU coverage in STVN.

Some challenges and up-to-date solutions are presented on topics, including SAGVN reconfiguration with dynamic space resource constraints, multidimensional sensing, and efficient integration of multidimensional context information, as well as real time, reliable, and secure communications for vehicles.

In most existing works, satellites have been assumed to exhibit a uniform distribution across the surface of a sphere, often following either the BPP or Poisson point process (PPP). However, it is essential to account for the impact of Earth's rotation-induced relative movement on communication performance. To address this gap, we present an analysis of LEO satellite communication performance in a practical satellite constellation with various constellation parameters. These parameters include orbit inclination, satellite boresight angle, ground user elevation angle, number of satellites on each orbit, and number of satellite orbits in the constellation. Additionally, it is crucial to investigate how different terrestrial network deployment strategies impact the enhancement of CAV network performance facilitated by LEO satellites.

B. Contributions

To explore the potential benefits of integrating LEO satellites with the terrestrial CAV networks, in this article, we consider an STVN where both LEO satellites and RSUs can provide network services for CAVs within their coverage, as shown in Fig. 1. Specifically, RSUs are connected to Internet-at-large through the terrestrial network. Satellites operate as regenerative relays, similar to a 3GPP radio access network distributed unit [12]. A satellite is connected to a CAV through a service link and coupled to a ground station through a feeder link. Note that our primary focus in this article is on the performance of service links. Specifically, we develop a practical LEO satellite constellation model for communication analysis. Based on the model, we investigate how key parameters of the satellite constellation affect propagation delay and network coverage in satellite-terrestrial communication. The LEO satellite-CAV network performance is theoretically analyzed in terms of network service availability, outage probability, and throughput. Furthermore, the STVN communication performance is analyzed when considering diversified terrestrial infrastructure deployment strategies. Extensive numerical results are provided to validate our theoretical analysis and demonstrate the performance advantage of the STVN. The main contributions of this article are summarized as follows.

- 1) We develop a practical LEO satellite communication model and analyze the impact of different satellite orbital parameters on the LEO satellite-CAV communication performance.
- 2) We comprehensively investigate the performance of LEO satellite-CAV communication, including service availability, outage probability, and system throughput, while considering practical satellite constellations.
- 3) We explore the STVN performance characteristics with different terrestrial infrastructure deployment strategies and evaluate how the integration of LEO satellites and terrestrial networks enhances the CAV service performance.

The remainder of this article is organized as follows. The LEO satellite constellation model is established and the impact of LEO satellite constellation parameters is investigated in Section II. In Section III, we analyze the performance of LEO satellite-CAV communication networks in terms of service availability, outage probability, and throughput. In Section IV, we study the impact of different LEO satellite constellations and different network deployment strategies on the communication performance. Numerical results are presented in Section V to corroborate our analysis on STVN performance with practical LEO satellite constellation. Finally, we conclude this study and discuss future works in Section VI.

II. LEO SATELLITE CONSTELLATION PARAMETERS

In this section, we first establish an LEO satellite constellation model, considering the impact of Earth rotation and the constraints of elevation and boresight angles. Then, we analyze the required number of satellites per satellite orbit and the number of orbits in the constellation to ensure uninterrupted satellite coverage. For clarity, we provide a summary of the primary notations used in this article in Table I.

A. Satellite Movement With Earth Rotation

Due to Earth's rotation, the movement of LEO satellites is not a simplistic circular motion relative to the ground observation point as assumed in most existing works. Fig. 2(a) shows the relative motion between satellites and ground. The blue orbit is the satellite orbit without considering Earth rotation. The red ones are the satellite orbits with Earth rotation, which are constantly changing relative to the Earth.

To further investigate the satellite movement and its impact on the LEO satellite-CAV communication performance, we consider an Earth-centered Earth-fixed (ECEF) coordinate system with the center of the Earth at its origin, as shown in Fig. 2(b), where the shape of the Earth is assumed as a perfect sphere.¹ Specifically, the $+x$ -axis passes through the Equator and Prime Meridian intersection, the $+z$ -axis passes through the North Pole, and the y -axis is orthogonal to x -axis

¹For more accurate modeling, we can approximate the Earth as an ellipsoid following the WGS84 model, with the rotation axis aligned with the rotation axis of the Earth. However, the comparison of LEO satellite-CAV distances between the WGS84 model and sphere model reveals negligible differences. Even in extreme cases, such as CAVs at the pole or equatorial areas, where discrepancies are the most prominent, the difference remains below 0.01%. Therefore, we model the Earth as a sphere for simplicity.

TABLE I
SUMMARY OF NOTATIONS

Notation	Definition
r_E, r	Earth radius and LEO satellite orbit radius
α, h	Satellite orbit inclination angle and orbit altitude
ϕ	Angle between a satellite and the ascending node
ω	Angle between the x -axis and the line from the origin to the ascending node
(β_u, γ_u)	(latitude, longitude) of a CAV
d	The distance between a CAV and its associated access point (LEO satellite or RSU)
θ_{th}	The minimum elevation angle constraint
μ_{th}	The maximum satellite boresight angle constraint
d_{max}	The maximum satellite-CAV distance to satisfy elevation angle and boresight angle constraints
N, M	No. of satellite orbits and No. of satellites per orbit
P_a^o	Probability of an LEO orbit being feasible for CAVs
P_a^s	Probability of at least one satellite on an orbit being available to provide CAV services
$P_{a,1}$	Probability of LEO-CAV service being available
$R_{t,1}$	Required throughput for satellite communications
$R_{t,2}$	Required throughput for terrestrial communications
λ_x	RSU deployment intensity in terrestrial RSU deployment Case x ($x \in \{a, b, c, d, e\}$)
$P_{o,1}$	Satellite communication service outage probability
$P_{o,2}^x$	Terrestrial service outage probability in RSU deployment Case x ($x \in \{a, b, c, d, e\}$)
$T_{1,max}$	Maximum achievable satellite system throughput
$T_{2,max}^x$	Maximum achievable terrestrial system throughput in RSU deployment Case x ($x \in \{a, b, c, d, e\}$)

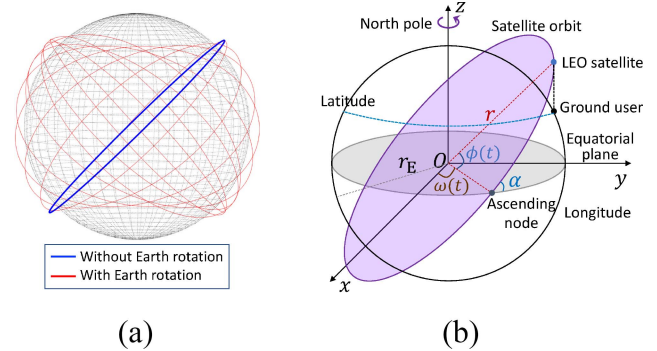


Fig. 2. Illustration of satellite orbits. (a) Satellite orbits with and without Earth rotation. (b) ECEF coordinate system.

and z -axis. This coordinate system rotates with the Earth. In Fig. 2(b), r is the LEO satellite orbit radius, which is the sum of Earth radius r_E and orbit altitude h , and α is the orbital inclination angle. The time-varying angle between the x -axis and the line from the origin to the ascending node is denoted by $\omega(t)$, given by

$$\omega(t) = \omega_0 + \Delta\omega_E \cdot t \quad (1)$$

where ω_0 is the initial angle of the ascending node, $\Delta\omega_E$ is the Earth rotation angular velocity, and $\Delta\omega_E \cdot t$ is the Earth rotation angle at time t . Let $\phi(t)$ be the time-varying angle between the satellite and the ascending node at time t , expressed as follows:

$$\phi(t) = \phi_0 + \Delta\phi_S \cdot t \quad (2)$$

where ϕ_0 is the initial angle between the satellite and ascending node, $\Delta\phi_S$ is the satellite rotation angular velocity,

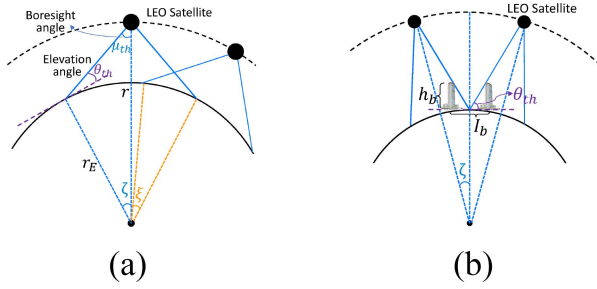


Fig. 3. Illustration of LEO satellite coverage. (a) Elevation angle and boresight angle constraints. (b) High-rise building blockage constraints.

and $\Delta\phi_s \cdot t$ is the satellite rotation angle along the orbit at time t .

Denote the latitude and longitude of a CAV on ground by β_u and γ_u , respectively. Therefore, the coordinate of the CAV in the coordinate system is transformed and given by

$$\begin{cases} x_u = r_E \cos \beta_u \cos \gamma_u \\ y_u = r_E \cos \beta_u \sin \gamma_u \\ z_u = r_E \sin \beta_u. \end{cases} \quad (3)$$

We represent the satellite coordinate as a function of time t , which is affected by the Earth rotation and satellite movement, given by

$$\begin{cases} x_s(t) = r \cos \phi(t) \cos \omega(t) - r \sin \phi(t) \sin \omega(t) \cos \alpha \\ y_s(t) = r \cos \phi(t) \sin \omega(t) + r \sin \phi(t) \cos \omega(t) \cos \alpha \\ z_s(t) = r \sin \phi(t) \sin \alpha. \end{cases} \quad (4)$$

The distance between an LEO satellite and the CAV can be calculated based on their coordinates as follows:

$$d(t) = \sqrt{(x_s(t) - x_u)^2 + (y_s(t) - y_u)^2 + (z_s(t) - z_u)^2}. \quad (5)$$

B. Impact of Elevation Angle and Boresight Angle

To satisfy the minimum elevation angle and satellite boresight angle constraints, the LEO satellite-CAV distance should satisfy the following relations:

$$d(t) \leq \sqrt{r^2 - r_E^2 + r_E^2 \sin^2 \theta_{th}} - r_E \sin \theta_{th} \quad (6a)$$

$$d(t) \leq r \cos \mu_{th} - \sqrt{r_E^2 - r^2 + r^2 \cos^2 \mu_{th}} \quad (6b)$$

where θ_{th} and μ_{th} are the minimum elevation angle and the maximum satellite boresight angle, respectively.

Note that in scenarios where satellite communications remain unobstructed (e.g., in rural areas), the minimum elevation angle constraint in (6a) and the maximum boresight angle constraint in (6b) are interrelated. In this case, as shown in Fig. 3(a), the minimum elevation angle can be determined by the maximum boresight angle of satellites, given by

$$\sin(\mu_{th}) = r_E \cos(\theta_{th})/r. \quad (7)$$

However, in city scenarios where high-rise buildings may block the satellite communication links, the minimum elevation angle is mainly affected by the building height and interbuilding distance, rather constrained by the satellite boresight angle. In a city scenario with a maximum building height

of h_d and a minimum interbuilding distance of I_d , as shown in Fig. 3(b), the minimum elevation angle should satisfy

$$\theta_{th} = \arctan(h_d/(0.5I_d)) \quad (8)$$

to guarantee that users between the buildings can be seamlessly covered by LEO satellites.

C. Number of Satellites on One Orbit

Next, we present the minimum number of LEO satellites on one orbit to guarantee that there is no coverage gap between adjacent satellites. Given the minimum elevation angle, θ_{th} , we can obtain the Earth central angle, ζ , as shown in Fig. 3(a). Here, ζ is the angle between the satellite and a CAV at the satellite coverage edge to the Earth center, given by

$$\zeta = \arcsin(d_{\max} \cos \theta_{th}/r) \quad (9)$$

where

$$d_{\max} = \min \left(\begin{aligned} &\sqrt{r^2 - r_E^2 + r_E^2 \sin^2 \theta_{th}} - r_E \sin \theta_{th} \\ &r \cos \mu_{th} - \sqrt{r_E^2 - r^2 + r^2 \cos^2 \mu_{th}} \end{aligned} \right)$$

is the maximum allowable satellite-CAV distance under elevation angle and boresight angle constraints. Then, the coverage area of one LEO satellite, denoted by S , is given by

$$S = 2\pi r_E^2 (1 - \cos \zeta). \quad (10)$$

To avoid coverage gap while satisfying the minimum elevation angle constraint, the minimum number of satellites on one orbit should satisfy

$$M_{\min} = \lceil \pi/\zeta \rceil. \quad (11)$$

When the number of LEO satellites on one orbit is larger than M_{\min} , for two adjacent satellites on the same orbit, the overlapped coverage angle, denoted by ξ , is expressed as follows:

$$\xi = 2\zeta - \frac{2\pi}{M_{\min}}. \quad (12)$$

D. Number of Orbits in Satellite Constellation

In this section, we study the required number of orbits in a satellite constellation to guarantee seamless coverage, which varies with the orbit inclination angle. We first consider polar orbits where the inclination angle is $(\pi/2)$, as shown in Fig. 4(a).

To guarantee seamless coverage, we need to ensure that CAVs on the equator can be served without interruption. Therefore, we consider the case that point A is on the equator. As analyzed in Section II-C, the angle between two adjacent satellites in the same orbit to the Earth center is $(2\pi/M_{\min})$. Therefore, the angle between a satellite and point A is $\angle s_1 OA = \angle s_2 OA = (\pi/M_{\min})$. To avoid coverage gaps, coverage areas of s_1 , s_2 , and s_3 should intersect at a common point I or exhibit a larger overlap area. In this case, satellite s_3 in the adjacent orbit must satisfy

$$\begin{aligned} \angle s_3 OA \leq \Delta + \zeta = &\arccos(1 - \cos(\pi/M_{\min}) + \cos \zeta) \\ &+ \arcsin(d_{\max} \cos \theta_{th}/r). \end{aligned} \quad (13)$$

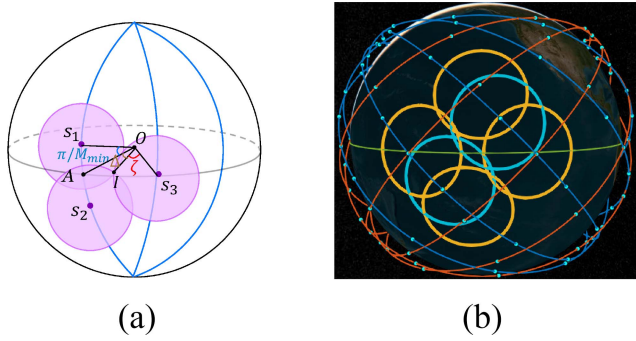


Fig. 4. LEO satellite coverage with different inclination angles. (a) Polar orbits ($\alpha = (\pi/2)$) (O : the Earth center. s_1 , s_2 , and s_3 : LEO satellites. A : the center of the coverage overlap area of s_1 and s_2 . I : the intersection of three satellites' coverage areas. The blue curves represent the satellite orbits, and the pink circles represent satellite coverage areas.) (b) Inclined orbits ($\alpha \neq (\pi/2)$). (Orange lines: ascending satellite orbits. Blue lines: descending satellite orbits. Green line: the Earth Equator. Yellow circles: the coverage areas of ascending satellites. Cyan circles: the coverage areas descending satellites.)

Considering the inherent symmetry of satellite orbits, if one side of the Earth can be seamlessly covered with ascending satellites, the complementary side will be seamlessly covered by descending satellites on the same orbits. Thus, we can obtain the minimum number of orbits, N_{\min} , for seamless coverage with polar orbit constellation as follows:

$$N_{\min} = \left\lceil \frac{\pi}{\arccos(1 - \cos(\frac{\pi}{M_{\min}})) + \cos \zeta + \arcsin(\frac{d_{\max}}{r} \cos \theta_{th})} \right\rceil. \quad (14)$$

Next, we consider inclined orbits with inclination angle $\alpha \neq \pi/2$. In inclined satellite constellation, both ascending satellites and descending satellites, moving in different directions, can provide coverage for the same region. Consider a satellite constellation with incline angle α , number of orbits N , the number of satellites per orbit M , and the relative phasing among satellites in different orbit planes F . At any given time instant, the position of a randomly chosen satellite in the satellite constellation can be denoted by (ω_0, ϕ_0) , $\omega_0 \in [0, 2\pi)$, $\phi_0 \in [0, 2\pi)$ using the ECEF coordinate system as shown in Fig. 2(b). Therefore, the ECEF coordinates of all satellites in the same constellation at the same time instant can be denoted by

$$(\omega_s, \phi_s) = \left(\left(\omega_0 + n \cdot \frac{2\pi}{N} \right) \bmod 2\pi, \left(\phi_0 + n \cdot \frac{2\pi F}{MN} + m \cdot \frac{2\pi}{M} \right) \bmod 2\pi \right) \quad (15)$$

where $n \in [0, N-1]$ and $m \in [0, M-1]$ denote the n th orbit and the m th satellite in an orbit.

For a given point A on the Earth, its ECEF coordinate can be represented as (ω_A, ϕ_A) , $\omega_A \in [0, 2\pi)$, $\phi_A \in [0, 2\pi)$. The XYZ coordinates of point A and a satellite with position (ω_s, ϕ_s) can be calculated based on (4). The Earth-centered angle between point A and satellite S is given by

$$\angle AOS = \arccos \left[(x_A x_s + y_A y_s + z_A z_s) / (r r_E) \right]. \quad (16)$$

Seamless coverage is achieved at any time instant if, for any (ω_0, ϕ_0) , the Earth-centered angle between any point A and the closest satellite is consistently smaller than ζ . The objective is to find the minimum number of orbits, N_{\min} to

achieve seamless coverage. Mathematically, this is represented as follows:

$$\begin{aligned} & \max_{\omega_0, \phi_0, \omega_A, \phi_A} \min_{\omega_s, \phi_s} \angle AOS \leq \zeta \\ & \equiv \min_{\omega_0, \phi_0, \omega_A, \phi_A} \max_{\omega_s, \phi_s} (x_A x_s + y_A y_s + z_A z_s) / (r r_E) \geq \cos \zeta. \end{aligned} \quad (17)$$

Letting $f = (x_A x_s + y_A y_s + z_A z_s) / (r r_E)$, we have

$$\begin{aligned} f &= \cos \alpha \sin(\omega_A - \omega_s) \sin(\phi_s - \phi_A) \\ &+ \cos(\omega_A - \omega_s) (\cos \phi_s \cos \phi_A + \cos^2 \alpha \sin \phi_s \sin \phi_A) \\ &+ \sin^2 \alpha \sin \phi_s \sin \phi_A. \end{aligned} \quad (18)$$

Taking partial derivatives of f with respect to ω_s , we get

$$\begin{aligned} \partial f / \partial \omega_s &= -\cos \alpha \sin(\phi_s - \phi_A) \cos(\omega_A - \omega_s) \\ &+ (\cos \phi_s \cos \phi_A + \cos^2 \alpha \sin \phi_s \sin \phi_A) \\ &\sin(\omega_A - \omega_s). \end{aligned} \quad (19)$$

The maximization condition of $\max_{\omega_s, \phi_s} f$ requires the partial derivatives to be equal to zero, derived as follows:

$$\begin{aligned} \partial f / \partial \omega_s \Big|_{\omega_s^*} &= \sin(\omega_A - \omega_s^* - \Theta) = 0 \\ \omega_s^* &= \omega_A - \Theta + 2k\pi, k \in \{0, 1\} \end{aligned} \quad (20)$$

where

$$\begin{aligned} \sin \Theta &= \Gamma_1 / \sqrt{\Gamma_1^2 + \Gamma_2^2}, \quad \cos \Theta = \Gamma_2 / \sqrt{\Gamma_1^2 + \Gamma_2^2}. \\ \Gamma_1 &= \cos \alpha \sin(\phi_s - \phi_A) \\ \Gamma_2 &= \cos \phi_s \cos \phi_A + \cos^2 \alpha \sin \phi_s \sin \phi_A. \end{aligned} \quad (21)$$

In this case, we can update the expression of f and the partial derivative of f with respect to ϕ_s as follows:

$$\begin{aligned} f \Big|_{\omega_s^*} &= \sqrt{(1 - \sin^2 \phi_s \sin^2 \alpha)(1 - \sin^2 \phi_A \sin^2 \alpha)} \\ &+ \sin^2 \alpha \sin \phi_s \sin \phi_A \\ \frac{\partial f}{\partial \phi_s} &= -\frac{\sin^2 \alpha \sin \phi_s \cos \phi_s \sqrt{1 - \sin^2 \phi_A \sin^2 \alpha}}{\sqrt{1 - \sin^2 \phi_s \sin^2 \alpha}} \\ &+ \sin^2 \alpha \sin \phi_A \cos \phi_s. \end{aligned} \quad (22)$$

Let ϕ_s^* satisfy that $(\partial f / \partial \phi_s) \Big|_{\phi_s^*} = 0$, we have

$$\begin{aligned} \sin^2 \alpha \cos \phi_s^* \left[\sin \phi_A \sqrt{1 - \sin^2 \phi_s^* \sin^2 \alpha} \right. \\ \left. - \sin \phi_s^* \sqrt{1 - \sin^2 \phi_A \sin^2 \alpha} \right] = 0. \end{aligned} \quad (23)$$

Considering that $\cos \phi_s^* = 0$ corresponds to the minimum values of f , we arrive at the equation for achieving the maximum value of f

$$\begin{aligned} \sin^2 \phi_A (1 - \sin^2 \phi_s^* \sin^2 \alpha) &= \sin^2 \phi_s^* (1 - \sin^2 \phi_A \sin^2 \alpha) \\ \phi_s^* &= \phi_A \quad \text{or} \quad \phi_s^* = \pi - \phi_A + 2k\pi, k \in \{0, 1\} \\ \begin{cases} \omega_s^* = \omega_A + 2k\pi, & \text{if } \phi_s^* = \phi_A + 2k\pi \\ \omega_s^* = \omega_A - \arcsin \frac{\cos \alpha \sin(2\phi_A)}{1 - \sin^2 \phi_A \sin^2 \alpha} + 2k\pi \\ & \text{if } \phi_s^* = \pi - \phi_A + 2k\pi \text{ \& } \cos^2 \alpha \sin^2 \phi_A - \cos^2 \phi_A \geq 0 \\ \omega_s^* = \omega_A - \left(\pi - \arcsin \frac{\cos \alpha \sin(2\phi_A)}{1 - \sin^2 \phi_A \sin^2 \alpha} \right) + 2k\pi \\ & \text{if } \phi_s^* = \pi - \phi_A + 2k\pi \text{ \& } \cos^2 \alpha \sin^2 \phi_A - \cos^2 \phi_A < 0. \end{cases} \end{aligned}$$

Therefore, (ω_s^*, ϕ_s^*) represents the ideal position of point A's closest satellite. As satellite positions are noncontinuous and fixed at a given time instant, as shown in (15), we aim to find the satellite (ω'_s, ϕ'_s) in the constellation that is closest to (ω_s^*, ϕ_s^*) . This is expressed as follows:

$$\begin{aligned} n' &= \text{round}[(\omega_s^* - \omega_0)N/2\pi] \\ m' &= \text{round}[(\phi_s^* - \phi_0 - n' \cdot 2\pi F/MN) \cdot M/2\pi] \\ \omega'_s &= (\omega_0 + n' \cdot 2\pi/N) \bmod 2\pi \\ \phi'_s &= (\phi_0 + n' \cdot 2\pi F/MN + m' \cdot 2\pi/M) \bmod 2\pi. \end{aligned} \quad (24)$$

The subsequent step involves determining $\min_{\omega_0, \phi_0, \omega_A, \phi_A} f|_{(\omega'_s, \phi'_s)}$. Due to the round operations in (24), optimizing this problem directly is challenging. To address this, we employ the linear search algorithm to find optimal values for $\omega_0, \phi_0, \omega_A$, and ϕ_A to minimize $f|_{(\omega'_s, \phi'_s)}$, denoted as f^* . Note that f^* is a function of N , and by ensuring $f^* \geq \cos \zeta$, we can readily identify the minimum number of orbits N_{\min} required to achieve seamless coverage.

III. STVN COMMUNICATION PERFORMANCE ANALYSIS

In this section, we analyze the impact of satellite orbit parameters on STVN communication performance in terms of service availability, outage probability, and throughput. Considering that vehicle mobility is negligible compared to LEO satellite movement, we mainly focus on the impact of satellite mobility in the performance analysis.

A. LEO Satellite-CAV Service Availability

Based on the analysis in Section II-A, the satellite coordinate is a function of $\omega(t)$ and $\phi(t)$. Thus, we can rewrite the time-varying LEO satellite-CAV distance as a function of ϕ and ω (omitting t for notational simplicity), given by

$$\begin{aligned} d(\phi, \omega) &= (r^2 + r_E^2 - 2r[x_u(\cos \phi \cos \omega - \sin \phi \sin \omega \cos \alpha) \\ &\quad + y_u(\cos \phi \sin \omega + \sin \phi \cos \omega \cos \alpha) + z_u \sin \phi \sin \alpha])^{0.5}. \end{aligned} \quad (25)$$

Given orbit inclination angle α and Earth rotation angle ω , the satellite orbit is known. For satellites on the orbit with different initial angles ϕ_0 , the distances between them and a given CAV are different. We can derive the shortest distance between the CAV to any point on the orbit by letting the derivative of the distance in terms of ϕ be zero, given by

$$\frac{\partial d(\phi, \omega)}{\partial \phi} = 0 \quad (26)$$

which leads to

$$\sin^2 \phi = \frac{1}{1 + \left(\frac{x_u \cos \omega + y_u \sin \omega}{z_u \sin \alpha - x_u \sin \omega \cos \alpha + y_u \cos \omega \cos \alpha} \right)^2}. \quad (27)$$

Letting $U = x_u \cos \omega + y_u \sin \omega$ and $Q = z_u \sin \alpha - x_u \sin \omega \cos \alpha + y_u \cos \omega \cos \alpha$, we have

$$\phi = \arcsin\left(Q/\sqrt{Q^2 + U^2}\right). \quad (28)$$

The minimum CAV-satellite distance, given α and ω , is

$$\begin{aligned} d_{\alpha, \omega}^{\min} &= \left(r^2 + r_E^2 - 2r[U \cos \phi + Q \sin \phi]\right)^{1/2} \\ &= \left(r^2 + r_E^2 - 2r\sqrt{Q^2 + U^2}\right)^{1/2}. \end{aligned} \quad (29)$$

If $d_{\alpha, \omega}^{\min} > d_{\max}$, the satellite orbit is not feasible, i.e., it is impossible for satellites on the orbit to satisfy the satellite-CAV communication distance constraint. The satellite orbit feasibility can be derived based on Proposition 1, the proof of which is given in Appendix A.

Proposition 1: Define U and Q as functions of ω , where $U = x_u \cos \omega + y_u \sin \omega$ and $Q = z_u \sin \alpha - x_u \sin \omega \cos \alpha + y_u \cos \omega \cos \alpha$. Denote the solutions to equation $Q^2 + U^2 = [(r^2 + r_E^2 - d_{\max}^2)/2r]^2$ by ω_1 and ω_2 . When there are N satellite orbits with maximum orbit separation, the probability of having at least one feasible satellite orbit is

$$P_a^o = \begin{cases} \frac{N|\omega_1 - \omega_2|}{\pi}, & \text{if } \alpha = \frac{\pi}{2} \text{ and } |\omega_1 - \omega_2| \leq \frac{\pi}{N} \\ 1, & \text{if } \alpha = \frac{\pi}{2} \text{ and } |\omega_1 - \omega_2| > \frac{\pi}{N} \\ \frac{N|\omega_1 - \omega_2|}{2\pi}, & \text{if } \alpha < \frac{\pi}{2} \text{ and } |\omega_1 - \omega_2| \leq \frac{2\pi}{N} \\ 1, & \text{if } \alpha < \frac{\pi}{2} \text{ and } |\omega_1 - \omega_2| > \frac{2\pi}{N}. \end{cases} \quad (30)$$

When an orbit is feasible (i.e., $\omega \in [\min(\omega_1, \omega_2), \max(\omega_1, \omega_2)]$), a satellite on the orbit is available to provide CAV services only when the communication distance constraint is satisfied. Thus, the range of ϕ should satisfy

$$d(\phi, \omega) \leq d_{\max}. \quad (31)$$

Letting $\mu = -x_u \sin \omega \cos \alpha + y_u \cos \omega \cos \alpha + z_u \sin \alpha$, $\nu = x_u \cos \omega + y_u \sin \omega$, and $\kappa = [(r^2 + r_E^2 - d_{\max}^2)/2r]$, we have

$$\mu \sin \phi + \nu \cos \phi \leq \kappa. \quad (32)$$

When there are M satellites on the orbit, the probability that at least one satellite on the orbit is available is given by

$$\begin{aligned} P_a^s &= \Pr(d(\phi, \omega) \leq d_{\max} | \omega) \\ &= \begin{cases} \frac{M|\phi_1 - \phi_2|}{2\pi} = \frac{M \cos^{-1}\left(\frac{\kappa}{\sqrt{\mu^2 + \nu^2}}\right)}{\pi}, & |\phi_1 - \phi_2| \leq \frac{M}{2\pi} \\ 1, & |\phi_1 - \phi_2| > \frac{M}{2\pi} \end{cases} \end{aligned} \quad (33)$$

where

$$\begin{aligned} \phi_1 &= -\cos^{-1}\left(\frac{\kappa}{\sqrt{\mu^2 + \nu^2}}\right) + \tan^{-1}\left(\frac{\mu}{\nu}\right) \\ \phi_2 &= \cos^{-1}\left(\frac{\kappa}{\sqrt{\mu^2 + \nu^2}}\right) + \tan^{-1}\left(\frac{\mu}{\nu}\right). \end{aligned}$$

Overall, the probability that LEO satellite-CAV service is available is given by

$$P_{a,1} = P_a^o \times P_a^s. \quad (34)$$

B. LEO Satellite-CAV Outage Probability

When satellite-CAV distance is smaller than d_{\max} , the elevation angle and boresight angle constraints are satisfied and the LEO satellite-CAV service is available. In addition, LEO satellite-CAV communications should satisfy throughput requirements. Service outage happens if the link capacity is smaller than the required throughput. Considering LEO satellite-CAV communications over an additive white Gaussian noise (AWGN) channel, the link capacity can be calculated using the Shannon formula, given by

$$C_1 = B_1 \log_2 \left(1 + \frac{G_{t,1} G_{r,1} P_1 c^2}{(4\pi f_1)^2 \sigma^2 d^2} \right) \quad (35)$$

where free-space path loss is assumed for LEO satellite-CAV communications. $G_{t,1}$, $G_{r,1}$, B_1 , p_1 , c , f_1 , and σ^2 denote the LEO satellite-CAV communication transmission antenna gain, receiving antenna gain, channel bandwidth, transmit power, light speed, carrier frequency, and noise power, respectively.

Proposition 2: Denote by $R_{t,1}$ the required LEO satellite-CAV throughput. When satellite-CAV distance is smaller than d_{\max} , the service outage probability is

$$P_{o,1} = \min \left(1, \max \left(0, \frac{d_{\max}^2 - \frac{G_{t,1}G_{r,1}p_1c^2}{(4\pi f_1)^2\sigma^2(2^{R_{t,1}/B_1} - 1)}}{d_{\max}^2 - h^2} \right) \right).$$

Proof: The service outage happens when the link capacity is smaller than the required throughput. Thus, we have

$$P_{o,1} = \Pr(C_1 \leq R_{t,1} \mid d \leq d_{\max}) = \Pr(d \geq d_{t,1} \mid d \leq d_{\max})$$

where

$$d_{t,1} = \sqrt{\frac{A_1}{(2^{R_{t,1}/B_1} - 1)}}, \quad A_1 = \frac{G_{t,1}G_{r,1}p_1c^2}{(4\pi f_1)^2\sigma^2}.$$

The LEO satellite-CAV distance should be less than $d_{t,1}$ to avoid service outage. Notice that the area of a spherical cap constrained by maximum distance x (i.e., the distance between all the points in the cap and the ground user does not exceed x) is $[(\pi(r_E + h)(x^2 - h^2))/(r_E)]$, where h is the satellite orbit altitude. Therefore, we have

$$P_{o,1} = \frac{\frac{\pi(r_E+h)(d_{\max}^2-h^2)}{r_E} - \frac{\pi(r_E+h)(d_{t,1}^2-h^2)}{r_E}}{\frac{\pi(r_E+h)(d_{\max}^2-h^2)}{r_E}} = \frac{d_{\max}^2 - d_{t,1}^2}{d_{\max}^2 - h^2}.$$

If $d_{t,1} < h$, none of the satellites in the orbit can satisfy the throughput requirement and the outage probability is $P_{o,1} = 1$. If $d_{t,1} > d_{\max}$, the throughput requirement can be satisfied as long as the elevation angle and boresight angle constraints are met, so we have $P_{o,1} = 0$. Overall, the satellite-CAV service outage probability is

$$P_{o,1} = \min \left(1, \max \left(0, \frac{d_{\max}^2 - d_{t,1}^2}{d_{\max}^2 - h^2} \right) \right).$$

C. LEO Satellite-CAV Throughput

With known LEO satellite-CAV service availability and outage probability, the achievable system throughput is defined as the data rate successfully transferred from the LEO satellite to the CAV without outage. For an LEO satellite-CAV link with a transmission rate of R , the achievable throughput is

$$T_1 = P_{a,1} \cdot (1 - P_{o,1}) \cdot R = \begin{cases} P_{a,1} \cdot R, & \text{if } R \in [0, R_{\max}^1] \\ P_{a,1} \cdot \frac{\frac{A_1}{R} - h^2}{\frac{2^{B_1} - 1}{d_{\max}^2 - h^2}} \cdot R, & \text{if } R \in [R_{\max}^1, R_{\max}^2] \\ 0, & \text{if } R \in [R_{\max}^2, \infty) \end{cases} \quad (36)$$

where $R_{\max}^1 = B_1 \log_2(1 + (A_1/d_{\max}^2))$ and $R_{\max}^2 = B_1 \log_2(1 + (A_1/h^2))$.

The maximum achievable throughput can be derived based on Proposition 3, the proof of which is given in Appendix B.

Proposition 3: For an LEO satellite-CAV link with a transmission rate of R , the maximum throughput is achieved when $R = B_1 \log_2(1 + (A_1/d_{\max}^2))$, which is

$$T_1 = P_{a,1}B_1 \log_2 \left(1 + \frac{A_1}{d_{\max}^2} \right).$$

When n CAVs are served by the same LEO satellite using orthogonal channels, the overall achievable throughput is

$$T_{1,n} = P_{a,1} \left(1 - \min \left(1, \max \left(0, \frac{d_{\max}^2 - d_{t,n}^2}{d_{\max}^2 - h^2} \right) \right) \right) \cdot R \cdot n \quad (37)$$

where

$$d_{t,n} = \sqrt{\frac{G_{t,1}G_{r,1}p_1c^2}{(4\pi f_1)^2\sigma^2(2^{nR_{t,1}/B_1} - 1)}} = \sqrt{\frac{A_1}{(2^{nR_{t,1}/B_1} - 1)}}.$$

In this case, the LEO satellite-CAV distance should be less than $d_{t,n}$ to avoid service outage. Similar to the preceding analysis, the maximum overall system throughput is achieved when $nR = B_1 \log_2(1 + (A_1/d_{\max}^2))$, given by

$$T_{1,\max} = P_{a,1}B_1 \log_2 \left(1 + \frac{A_1}{d_{\max}^2} \right). \quad (38)$$

IV. STVN PERFORMANCE WITH DIFFERENT TERRESTRIAL NETWORK DEPLOYMENT STRATEGIES

Based on the performance analysis on LEO satellite-CAV communications, we further study the STVN performance with different terrestrial network deployment strategies.

A. Terrestrial Network Deployment Strategies

In terrestrial CAV networks, RSU deployment may be affected by road layouts. Here, we consider two different road layouts, as shown in Fig. 5. Fig. 5(a) shows a scenario where roads are parallel with an equal distance of ϱ , and Fig. 5(b) shows crossed roads with an equal distance of ϱ . We consider three different terrestrial RSU deployment strategies.

- 1) *1-D PPP*: RSUs are deployed along roads following 1-D PPP distributions.
- 2) *1-D Equal Interval Deployment*: RSUs are deployed along roads with equal distance separations.
- 3) *2-D PPP*: For performance comparison, we further consider the scenario where RSUs or cellular base stations (BSs) are not deployed along roads [27]. For description consistency, we use the term RSUs in the following to represent both the traditional RSUs and cellular BSs. In this case, RSUs are randomly deployed in a 2-D area following a PPP distribution, independent of the road layout.

Combining different road layouts and RSU deployment strategies, we have five terrestrial RSU deployment cases.

- 1) *Case a*: 2-D PPP RSU deployment with intensity λ_a .
- 2) *Case b*: 1-D PPP RSU deployment in parallel roads with intensity λ_b .
- 3) *Case c*: 1-D PPP RSU deployment in crossed roads with intensity λ_c .

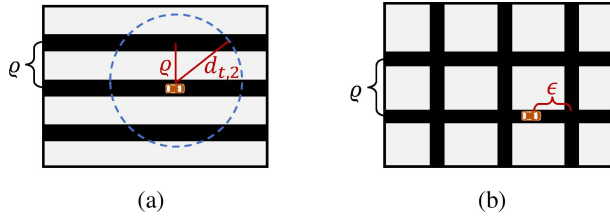


Fig. 5. Two different road layouts. (a) Parallel roads. (b) Crossed roads.

- 4) *Case d*: 1-D equal interval RSU deployment in parallel roads with intensity λ_d .
- 5) *Case e*: 1-D equal interval RSU deployment in crossed roads with intensity λ_e .

In case a, the probability of x terrestrial RSUs in a unit area is $[(\lambda_d^x)/x!]e^{-\lambda_d}$ and the probability of no RSUs within area of size ζ is $e^{-\lambda_d\zeta}$. In case b and case c, the probabilities of no RSU in a road segment of length l are $e^{-\lambda_b l}$ and $e^{-\lambda_c l}$, respectively. In case d and case e, the distance separations of adjacent RSUs are $l_d = [1/(\lambda_d)]$ and $l_e = [1/(\lambda_e)]$, respectively. Let

$$f(\lambda, l) = \max\left(0, \frac{1/\lambda - l}{1/\lambda}\right). \quad (39)$$

The probabilities of no RSU in a road segment of length l in case d and case e are $f(\lambda_d, l)$ and $f(\lambda_e, l)$, respectively.

B. Service Outage Probability and Throughput

Considering terrestrial CAV communications over an AWGN channel, the achievable link capacity is calculated using the Shannon formula, given by

$$C_2 = B_2 \log_2 \left(1 + \frac{G_{t,2} G_{r,2} p_2 c^2}{(4\pi f_2)^2 \sigma^2 d^{\alpha_P}}\right) \quad (40)$$

where $G_{t,2}$, $G_{r,2}$, B_2 , p_2 , f_2 , α_P , and σ^2 denote the terrestrial CAV communication transmission antenna gain, receiving antenna gain, channel bandwidth, transmit power, carrier frequency, path-loss exponent, and noise power, respectively.

To satisfy a given target terrestrial data rate $R_{t,2}$, we have

$$C_2 \geq R_{t,2}. \quad (41)$$

Thus, the RSU-CAV communication distance should satisfy

$$d \leq d_{t,2} = \left(\frac{A_2}{2^{R_{t,2}/B_2} - 1}\right)^{\frac{1}{\alpha_P}} \quad (42)$$

where

$$A_2 = \frac{G_{t,2} G_{r,2} p_2 c^2}{(4\pi f_2)^2 \sigma^2}. \quad (43)$$

For a CAV, the terrestrial service outage happens when no RSU is available within a distance of $d_{t,2}$. Note that for 1-D RSU deployment along roads, all possible network services from adjacent roads should be taken into account. Therefore, the service outage probabilities for different RSU deployment cases are, respectively, derived as follows:

$$P_{o,2}^a = e^{-\lambda_a \pi d_{t,2}^2} \quad (44a)$$

$$P_{o,2}^b = e^{-2\lambda_b d_{t,2}} \prod_{i=1}^{\lfloor d_{t,2}/\varrho \rfloor} e^{-4\lambda_b \sqrt{d_{t,2}^2 - (i\varrho)^2}} \quad (44b)$$

$$P_{o,2}^c = e^{-2\lambda_c d_{t,2}} \prod_{i=1}^{\lfloor d_{t,2}/\varrho \rfloor} e^{-4\lambda_c \sqrt{d_{t,2}^2 - (i\varrho)^2}} \quad (44c)$$

$$\times \int_0^\varrho \frac{1}{\varrho} \left(\prod_{i=0}^{\lfloor \frac{d_{t,2}-\epsilon}{\varrho} \rfloor} e^{-2\lambda_c \sqrt{d_{t,2}^2 - (i\varrho + \epsilon)^2}} \times \prod_{i=1}^{\lfloor \frac{d_{t,2} + \epsilon}{\varrho} \rfloor} e^{-2\lambda_c \sqrt{d_{t,2}^2 - (i\varrho - \epsilon)^2}} \right) d\epsilon$$

$$P_{o,2}^d = f(\lambda_d, 2d_{t,2}) \prod_{i=1}^{\lfloor \frac{d_{t,2}}{\varrho} \rfloor} \left(f\left(\lambda_d, 2\sqrt{d_{t,2}^2 - (i\varrho)^2}\right) \right)^2 \quad (44d)$$

$$P_{o,2}^e = f(\lambda_e, 2d_{t,2}) \prod_{i=1}^{\lfloor \frac{d_{t,2}}{\varrho} \rfloor} \left(f\left(\lambda_e, 2\sqrt{d_{t,2}^2 - (i\varrho)^2}\right) \right)^2 \quad (44e)$$

$$\times \int_0^\varrho \frac{1}{\varrho} \left(\prod_{i=0}^{\lfloor \frac{d_{t,2}-\epsilon}{\varrho} \rfloor} f\left(\lambda_e, 2\sqrt{d_{t,2}^2 - (i\varrho + \epsilon)^2}\right) \right.$$

$$\left. \times \prod_{i=1}^{\lfloor \frac{d_{t,2} + \epsilon}{\varrho} \rfloor} f\left(\lambda_e, 2\sqrt{d_{t,2}^2 - (i\varrho - \epsilon)^2}\right) \right) d\epsilon$$

where $f(\lambda, l)$ is given in (39).

The average throughput of a terrestrial CAV link is the data rate successfully transferred from the RSUs to the CAV without any outage. In case a, when there are n CAVs served by an RSU with a transmission rate of R , the average overall achievable throughput is

$$T_2^a = nR \left(1 - e^{-\lambda_a \pi \left(\frac{A_2}{2^{R/n} - 1}\right)^{\frac{2}{\alpha_P}}}\right). \quad (45)$$

Letting $x = nR$, T_2^a is a concave function of x . Therefore, the optimal value of x and the corresponding optimal overall throughput can be found by letting the first derivative equal to 0, given by

$$\frac{d T_2^a}{dx} = 1 - e^{-\lambda_a \pi \left(\frac{A_2}{2^{x/B_2} - 1}\right)^{\frac{2}{\alpha_P}}} \times \left(1 + \frac{x 2\lambda_a \pi A_2^{\frac{2}{\alpha_P}} \ln 2}{\alpha_P B_2} \frac{2^{\frac{x}{B_2}}}{\left(2^{\frac{x}{B_2}} - 1\right)^{\frac{2}{\alpha_P} + 1}}\right) = 0 \quad (46)$$

where the solution can be obtained by using computing software tools such as MATLAB toolboxes. The corresponding maximum achievable throughput is denoted by $T_{2,\max}^a$. The maximum achievable terrestrial throughput in cases b–e can be computed in the same manner.

Consider that satellite and terrestrial networks operate on different frequency bands. Then, the overall service availability in the STVN is

$$P_a = 1 - P_{o,2}^x \times (1 - P_{a,1} \cdot (1 - P_{o,1})) \quad (47)$$

TABLE II
SIMULATION PARAMETERS

LEO Satellite Orbital Parameters	
Orbit altitude	550 km
Number of satellites on one orbit	20
Initial angles (ω_0, ϕ_0)	(0,0)
Earth rotation angular velocity $\Delta\omega_E$	7.292×10^{-5} rad/s
Velocity of the satellite on its orbit	7.62 km/s
Default CAV location	$(\beta_u, \gamma_u) = (0, 0)$
LEO Satellite Communication Parameters [28]	
Carrier frequency f_1	20 GHz
Bandwidth B_1	500 MHz
Transmission power p_1	10 W
Noise power σ^2	-117 dBW
Antenna gains $G_{t,1}$ and $G_{r,1}$	32 dBi and 34 dBi
Terrestrial Communication Parameters [29]	
Carrier frequency f_2	28 GHz
Bandwidth B_2	200 MHz
Transmission power p_2	28 dBm
Path-loss exponent α_P	3
Antenna gains $G_{t,2}$ and $G_{r,2}$	3 dBi and 3 dBi

in terrestrial RSU deployment *Case x* ($\mathbf{x} \in \{\mathbf{a}, \mathbf{b}, \mathbf{c}, \mathbf{d}, \mathbf{e}\}$). The overall achievable STVN throughput is the sum of satellite network throughput and terrestrial throughput, given by

$$T = T_{1,\max} + T_{2,\max}^{\mathbf{x}} \quad (48)$$

in terrestrial RSU deployment *Case x* ($\mathbf{x} \in \{\mathbf{a}, \mathbf{b}, \mathbf{c}, \mathbf{d}, \mathbf{e}\}$).

V. PERFORMANCE EVALUATION

In this section, we conduct extensive simulations to evaluate the impact of different LEO satellite orbital parameters and terrestrial network deployment strategies on the STVN communication performance. The default simulation parameters are given in Table II.

A. Impact of LEO Satellite Orbital Parameters

First, we investigate the impact of Earth rotation on the propagation delay and satellite coverage duration, where CAVs always choose the closest satellite for connection. As shown in Fig. 6(a), the CAV is located at $(\beta_u, \gamma_u) = (0, 0)$. When Earth rotation is ignored, the propagation delay varies regularly with the same amplitude when different satellites on the same orbit pass above the CAV. Since 20 satellites on one orbit can guarantee no coverage gap between adjacent satellites in both cases with elevation angles equal to 10° and 20° , different values of θ_{th} do not affect the propagation delay. On the other hand, when considering the Earth rotation, the experienced propagation delay varies for different LEO satellites on the same orbit. Specifically, the dashed line segments represent that the CAV is not covered by any satellite on the orbit. This means that the CAV may move beyond the coverage area of all satellites due to Earth rotation. In addition, with a smaller θ_{th} , the satellite coverage duration increases. When the CAV location is $(\beta_u, \gamma_u) = (\pi/4, \pi/4)$, we have similar observations, as shown in Fig. 6(b). Without Earth rotation,

the experienced propagation delay for successive satellites on the same orbit is the same. Otherwise, with Earth rotation, the experienced delay changes, and the variation has a period of one day due to the Earth rotation cycle.

Fig. 7 shows the impact of satellite orbital inclination and connection delay requirements on LEO satellite coverage duration. Specifically, the term “connected” means that CAVs are covered by LEO satellites once the elevation and boresight angle constraints are satisfied. Besides these constraints, different CAV services may have different delay requirements. Here, “<5 ms” and “<3 ms” represent that satellite services are available only when the propagation delay is less than 5 and 3 ms, respectively. Comparing Fig. 7(a) and (b), we can see that with the same satellite constellation, the coverage duration varies significantly for different CAV locations. For a CAV located at (0, 0), the coverage duration decreases when the inclination angle increases with Earth rotation. For a CAV located at $(\pi/4, \pi/4)$, it can get served only with some specific inclination angles. When considering the impact of Earth rotation, the practical LEO satellite coverage duration is much smaller than the ideal case without considering Earth rotation.

Fig. 8 shows the impact of the number of orbits and satellites per orbit on the propagation delay in different satellite constellations. Our analysis in Sections II-C and II-D reveals that for polar orbits, seamless coverage requires 9 satellite orbits with 13 satellites on each orbit. Similarly, for inclined orbits with $\alpha = \pi/4$, 7 orbits with 13 satellites on each orbit are necessary. As shown in Fig. 8(a), ensuring a consistent connection to satellites with varying propagation delay is achieved with 9 satellite orbits and 13 satellites per orbit. However, reducing the number of orbits to 8 or the number of satellites per orbit to 12 results in time intervals where the LEO-CAV propagation delay equals 0, indicating a loss of connectivity. Similarly, in Fig. 8(b), when the number of orbits or satellites per orbit falls below the required number based on our analysis (e.g., with 11 orbits or 13 satellites per orbit), seamless coverage cannot be achieved. These observations validate our analysis on the required number of orbits and satellites per orbit for seamless coverage.

In Fig. 9, we present the number of satellites required on each orbit and the maximum propagation delay performance with different elevation angles and overlapped angles. Specifically, the required number of satellites on each orbit to avoid coverage gap is shown on top of each bar in the figure. As shown in the figure, when the elevation angle constraint θ_{th} is small, which happens when there is little or no blockage on satellite communication links (e.g., in rural scenarios), the maximum propagation delay is relatively large and the required number of satellites on each orbit is small. When θ_{th} increases, which may be the result of high-rise building blockage in city scenarios, the coverage area of each satellite decreases, thus more satellites are required on each orbit and the experienced propagation delay decreases. Similarly, when the satellite coverage overlap angle [i.e., ξ as expressed in (12)] increases, the required number of satellites increases and the propagation delay decreases.

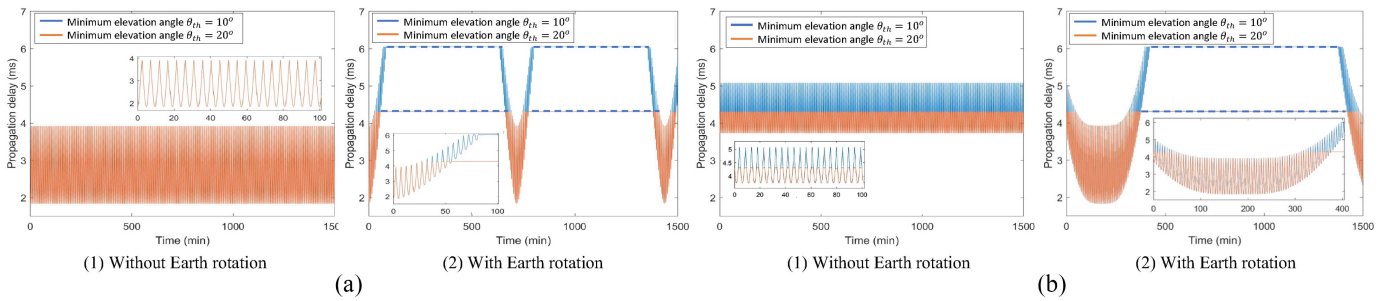


Fig. 6. LEO satellite-CAV communication propagation delay with and without Earth rotation (with inclination angle of $\pi/4$). (a) CAV location: $(\beta_u, \gamma_u) = (0, 0)$. (b) CAV location: $(\beta_u, \gamma_u) = (\pi/4, \pi/4)$.

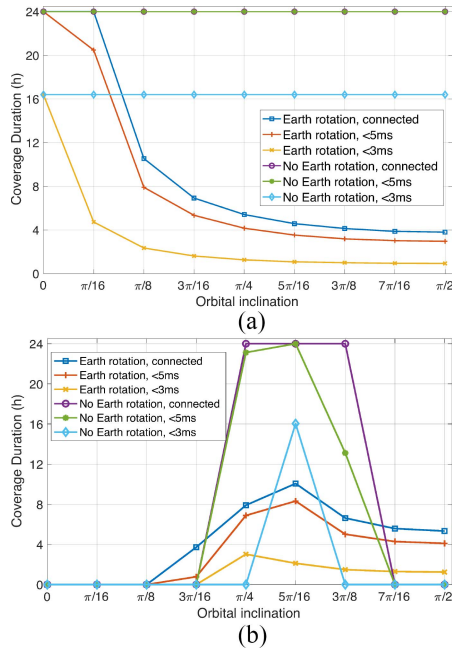


Fig. 7. Satellite coverage duration affected by Earth rotation. (a) CAV location: $(\beta_u, \gamma_u) = (0, 0)$. (b) CAV location: $(\beta_u, \gamma_u) = (\pi/4, \pi/4)$.

Next, the impact of different orbit numbers and satellite numbers on the coverage duration in each day is shown in Fig. 10. Specifically, a CAV is considered to be covered by an LEO satellite only when the propagation delay is less than 3 ms. When the orbit number is small, adding a new orbit is more effective in increasing the coverage duration than adding a new satellite in each orbit. For example, in Fig. 10(a), when the orbit number is 9, increasing the orbit number leads to larger coverage duration enhancement than adding one satellite on the same orbit. Nevertheless, when the orbit number is relatively large, adding a new satellite in each orbit is a more effective way to increase the coverage duration.

B. Performance of LEO Satellite-CAV Communications

We investigate the LEO satellite-CAV communication performance in terms of service availability, outage probability, and system throughput with different satellite constellation parameters. Fig. 11 shows the LEO satellite-CAV service availability with different orbit inclination angles and CAV latitudes. As shown in Fig. 11(a), polar orbits provide better coverage for users in high latitudes. With an increasing number

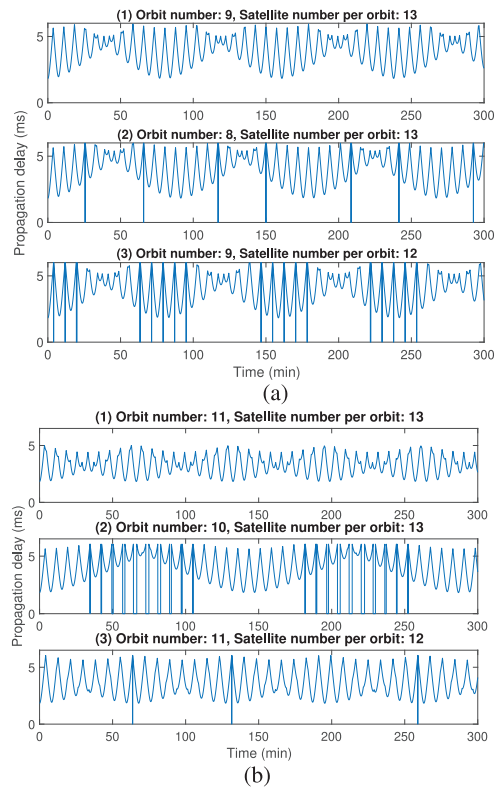


Fig. 8. Validation on the required number of orbits and satellites per orbit (CAV location: $(\beta_u, \gamma_u) = (0, 0)$). (a) Polar orbits $\alpha = \pi/2$. (b) Inclined orbits $\alpha = \pi/4$.

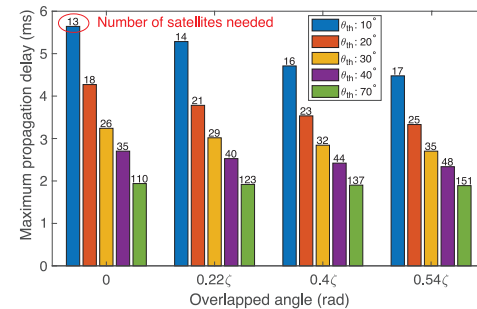


Fig. 9. Number of satellites required on each orbit and the maximum propagation delay with different elevation angles and overlapped angles (at orbital inclination angle of $\pi/2$).

of orbit planes, service availability increases. Fig. 11(b) shows that, with an orbit inclination angle of 53° , the inclined orbits provide better coverage for users in low latitudes than the polar

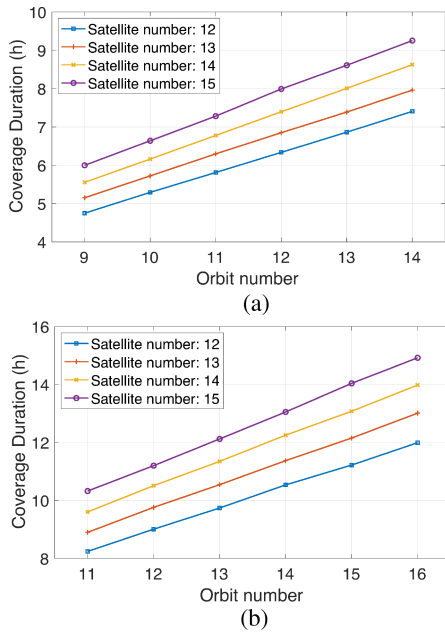


Fig. 10. LEO satellite coverage duration with different orbit numbers and satellite numbers. (a) Orbit inclination angle $\alpha = (\pi/2)$. (b) Orbit inclination angle $\alpha = (\pi/4)$.

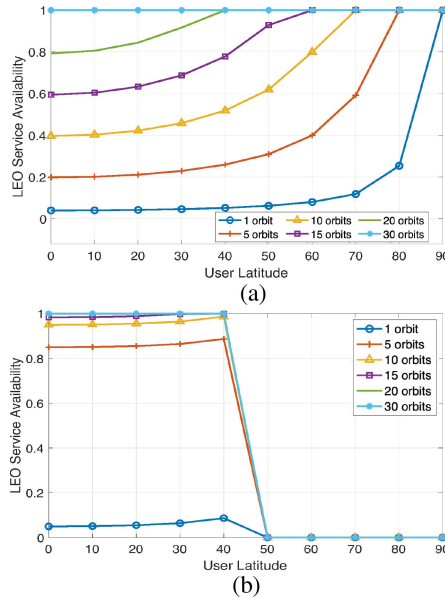


Fig. 11. LEO satellite-CAV communication service availability with different orbit inclination angles and CAV latitudes. (a) Polar orbits ($\alpha = (\pi/2)$). (b) Inclined orbits ($\alpha = 53^\circ$).

orbits. Therefore, to achieve high service availability in both high-latitude and low-latitude areas, a combination of polar orbits and inclined orbits should be adopted.

Fig. 12 shows the impact of the minimum required elevation angle θ_{th} and required satellite communicate data rate $R_{t,1}$ on the service outage probability. Given θ_{th} , the LEO satellite-CAV service outage probability increases with $R_{t,1}$, as a larger $R_{t,1}$ represents a stricter requirement on the LEO satellite-CAV communication distance. On the other hand, given $R_{t,1}$, both LEO satellite-CAV service outage probability and the service availability decrease when θ_{th} increases. When $R_{t,1}$ is smaller

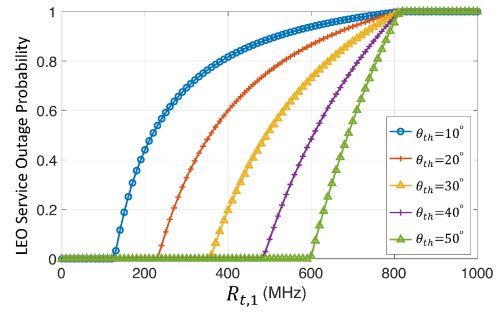


Fig. 12. LEO satellite-CAV outage probability with different elevation angle and data rate requirements ($\alpha = 53^\circ$).

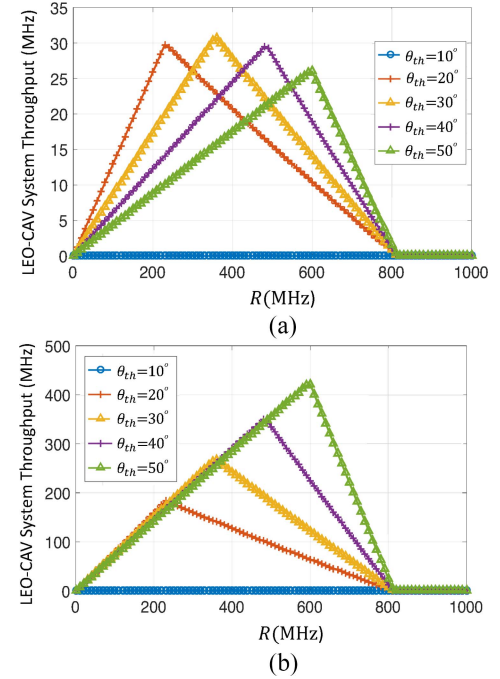


Fig. 13. LEO satellite-CAV communication throughput with different values of θ_{th} and R . (a) One inclined orbit ($\alpha = 53^\circ$). (b) Three inclined orbits ($\alpha = 53^\circ$).

than a certain threshold, the outage probability is 0; when $R_{t,1}$ is too large, the outage probability is 1. The observations conform to our analysis in Section III-B.

Fig. 13 shows the LEO satellite-CAV throughput performance with different values of θ_{th} and R . The throughput first increases and then decreases with R , consistent with our theoretical analysis. When R is small, the transmitted data rate is low; when R is large, the outage probability rises; both leading to a low throughput. With a small θ_{th} value, the outage probability is high, as presented in Fig. 12. If the value of θ_{th} is high, the satellite available probability (reflected by the slope of the increasing part of the curve) reduces. Both cases lead to a decreased throughput. Comparing Fig. 13(a) and (b), when the orbit number increases, the satellite available probability increases, and the impact of θ_{th} on satellite available probability reduces, resulting in a higher overall throughput. Therefore, the values of R and θ_{th} should be carefully determined to maximize the overall throughput.

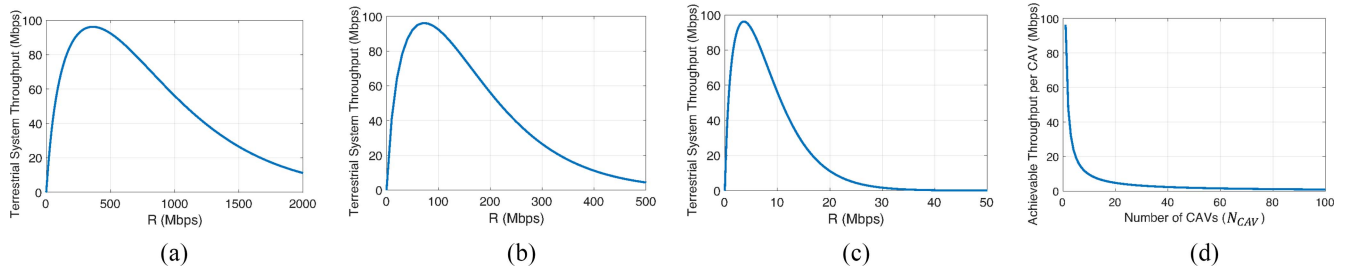


Fig. 14. Terrestrial CAV network throughput performance (case a: 2-D PPP RSU deployment with intensity $\lambda_a = 5 * 10^{-5}$). (a) $n = 1$. (b) $n = 5$. (c) $n = 100$. (d) Throughput per CAV.

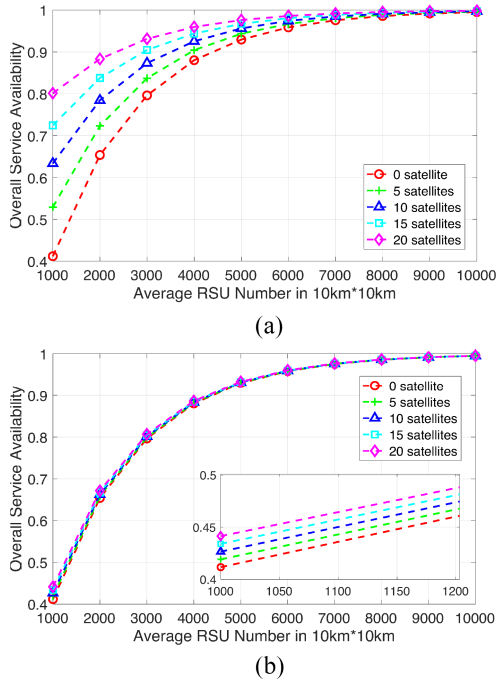


Fig. 15. Impact of RSU deployment intensities (case a), numbers of satellites, and elevation angle constraints on the overall service availability in STVN. (a) Elevation angle constraint $\theta_{th} = 30^\circ$. (b) Elevation angle constraint $\theta_{th} = 70^\circ$.

C. Impact of Terrestrial Network Deployment Strategies on STVN Performance

We investigate the impact of terrestrial network deployment strategies on STVN communication performance in the following simulations. The LEO satellite orbit number is 3, orbit inclination angle is 53° , and minimum elevation angle is 30° , unless specified otherwise.

Fig. 14 shows the terrestrial CAV network throughput with different values of transmission rate, R , and number of CAVs, n . As shown in Fig. 14(a)–(c), with different numbers of CAVs served by one terrestrial RSU, the optimal transmission rate for each CAV varies, but the overall terrestrial system throughput remains the same. As shown in Fig. 14(d), with more CAVs served by one RSU, the achievable throughput per CAV decreases as expected.

Fig. 15 shows the STVN service availability with different RSU deployment intensities, numbers of satellites, and elevation angles. With more RSUs deployed and more satellites in each orbit, the overall service availability increases. It is worth

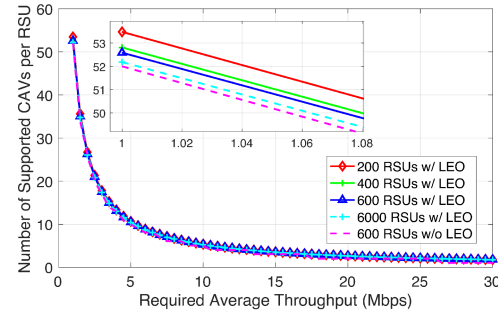


Fig. 16. Average number of supported CAVs per RSU versus the required average throughput for different numbers of RSUs covered by each LEO beam (case a with RSU deployment intensity $\lambda_a = 5 * 10^{-5}$).

noting that, with a low RSU deployment intensity and small θ_{th} , which can be regarded as a rural scenario with limited terrestrial infrastructure deployment and little blockage, the service availability improvement brought by LEO satellites is significant. On the other hand, with dense RSU deployment and a large θ_{th} , which can be regarded as a city scenario in which satellite communications in low elevation angles are blocked by high-rise buildings, the service availability improvement brought by LEO satellites is marginal.

Fig. 16 shows the average number of supported CAVs within each RSU coverage versus the required average throughput for different LEO satellite beam coverage. Different curves in the figure represent that one LEO satellite beam covers different numbers of RSUs, and the dashed pink curve represents the result without the LEO satellite. It is observed that, with the LEO satellite, the average number of supported CAVs per RSU increases. Moreover, with a larger beam coverage, fewer CAVs can be supported within each RSU area since the LEO satellite has limited overall throughput.

Next, we consider a fixed LEO beam coverage of 700 km^2 , where the radius of the beam is about 15 km. Within the beam coverage, the average number of CAVs supported per RSU for different RSU intensities versus the required average throughput is shown in Fig. 17. With a larger intensity of RSU deployment, which means more RSUs in an LEO satellite beam coverage, the average number of supported CAVs per RSU increases accordingly. With a higher required average throughput, fewer CAVs can be supported in the STVN.

In the following, we compare the STVN performance in different RSU deployment cases (i.e., case a—case e). For fair

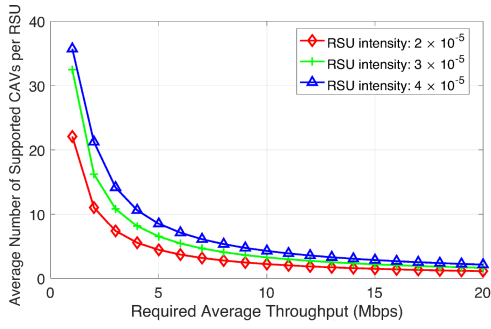


Fig. 17. Average number of supported CAVs per RSU versus the required average throughput (RSU deployment case a with the LEO satellite beam coverage area being 700 km^2).

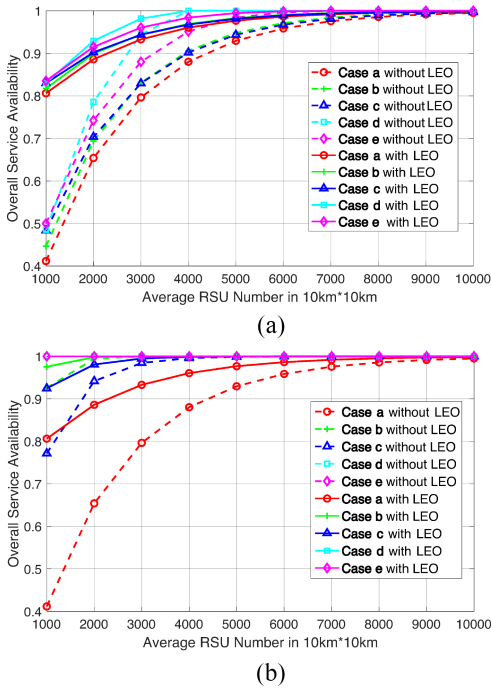


Fig. 18. Overall service availability in STVN with different RSU deployment strategies and intensities (CAVs are always on roads, LEO satellite orbit number: 20). (a) Road interval $\varrho = 100 \text{ m}$. (b) Road interval $\varrho = 1000 \text{ m}$.

comparison, we consider that the average number of RSUs in the target square area s^2 is n_R and will keep the same for different deployment strategies. Therefore, the respective RSU deployment intensities are

$$\lambda_a = \frac{n_R}{s^2}, \quad \lambda_b = \lambda_d = \frac{n_R \cdot \varrho}{s^2}, \quad \lambda_c = \lambda_e = \frac{n_R \cdot \varrho}{s^2}.$$

Fig. 18 shows the overall service availability in the STVN where all CAVs are on roads. Fig. 18(a) shows the service availability with the distance between adjacent roads being 100 m , which can be regarded as a city scenario with high-density roads. Fig. 18(b) shows a low-density road scenario, with the distance between adjacent roads being 1000 m . For all the RSU deployment cases without LEO satellites, the service availability varies significantly for different RSU deployment intensities. By adding LEO satellites, the service availability can be significantly improved. Specifically, the service availability improvement is more significant for cases

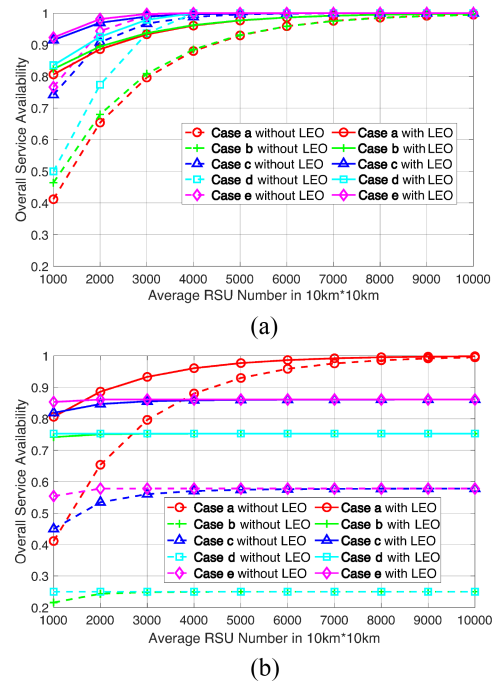


Fig. 19. Overall service availability in STVN with different RSU deployment strategies and intensities (CAVs are not always on roads, LEO satellite orbit number: 20). (a) Road interval $\varrho = 100 \text{ m}$. (b) Road interval $\varrho = 1000 \text{ m}$.

with smaller RSU intensities. From the results, 1-D RSU deployment (i.e., Cases b–e) performs well since all RSUs are deployed along roads to effectively serve on-road vehicles. On the other hand, 2-D PPP deployment (i.e., Case a) achieves low service availability especially in low-density road scenarios, since some RSUs may not be able to serve on-road vehicles. With increasing number of RSUs, the service availability increases significantly, and the LEO satellite can improve the overall service availability especially with a small number of RSUs.

Next, we consider a more general case that CAVs are not necessary to be always on roads. The related scenarios include parking spots or airports without clear road layouts, or dense urban scenarios where RSUs are only deployed along the major roads. As shown in Fig. 19(a), when the road density is high, 1-D on-road deployments [i.e., Cases b–e] achieve higher service availability than 2-D deployment since most vehicles can be served within the coverage of RSUs. However, the 1-D deployment performs worse than the 2-D deployment in low-density road scenarios, as shown in Fig. 19(b). This is because RSUs with 2-D PPP deployment can better serve vehicles not on roads, whereas RSUs with 1-D deployment can only serve limited areas near roads.

VI. CONCLUSION AND FUTURE WORK

In this article, theoretical models of LEO satellite-CAV communication have been developed. Considering different LEO satellite constellation parameters and terrestrial infrastructure deployment strategies, the service availability, outage probability, and throughput performance of the STVN have been investigated. Our theoretical analysis, supported by

numerical evaluation results, provides valuable insights into the performance improvement benefiting from LEO satellites with practical satellite and terrestrial network settings. This article can also provide useful guidelines for future studies related to LEO satellite-assisted networks. For future studies, we plan to extend our analysis by incorporating feeder links to explore the end-to-end LEO satellite-CAV communication performance. In addition, we will design cooperative service provisioning schemes for terrestrial RSUs and satellites to optimally decide whether and when to involve satellite communications.

APPENDIX A PROOF OF PROPOSITION 1

The probability of a satellite orbit being feasible (i.e., the minimum CAV-satellite distance can satisfy the maximum allowable distance constraint) is given by

$$\begin{aligned} P_a^o &= \Pr(d_{\alpha,\omega}^{\min} \leq d_{\max}) \\ &= \Pr\left(Q^2 + U^2 \geq \left(\frac{r^2 + r_E^2 - d_{\max}^2}{2r}\right)^2\right). \end{aligned}$$

When $\alpha = (\pi/2)$, we have $U = x_u \cos \omega + y_u \sin \omega$ and $Q = z_u$. Therefore, we have

$$\begin{aligned} U^2 + Q^2 &= x_u^2 - x_u^2 \sin^2 \omega + y_u^2 \sin^2 \omega + 2x_u y_u \cos \omega \sin \omega + z_u^2 \\ &= x_u y_u \sin 2\omega + \frac{x_u^2 - y_u^2}{2} \cos 2\omega + \frac{r_E^2 + z_u^2}{2} \\ &\geq \left(\frac{r^2 + r_E^2 - d_{\max}^2}{2r}\right)^2. \end{aligned}$$

Note that the solution to $\mu \sin x + \nu \cos x = \kappa$ is $x = 2n\pi \pm \cos^{-1}([\kappa/(\sqrt{\mu^2 + \nu^2})] + \tan^{-1}(\mu/\nu))$. Letting $\mu = x_u y_u$, $\nu = [(x_u^2 - y_u^2)/2]$, and $\kappa = [(r^2 + r_E^2 - d_{\max}^2)/2r]^2 - [(r_E^2 + z_u^2)/2]$, we can derive the two solutions, denoted by ω_1 and ω_2 , to the equation $Q^2 + U^2 = ((r^2 + r_E^2 - d_{\max}^2)/2r)^2$ as follows:

$$\begin{aligned} \omega_1 &= -\frac{1}{2} \left(\cos^{-1} \left(\frac{\kappa}{\sqrt{\mu^2 + \nu^2}} \right) + \tan^{-1} \left(\frac{\mu}{\nu} \right) \right) \\ \omega_2 &= \frac{1}{2} \left(\cos^{-1} \left(\frac{\kappa}{\sqrt{\mu^2 + \nu^2}} \right) + \tan^{-1} \left(\frac{\mu}{\nu} \right) \right). \end{aligned}$$

In general, for inclined orbits with $\alpha < \pi/2$, equation $Q^2 + U^2 = ((r^2 + r_E^2 - d_{\max}^2)/2r)^2$ also has two solutions ω_1 and ω_2 . Only when $\omega \in [\min(\omega_1, \omega_2), \max(\omega_1, \omega_2)]$, it is possible that satellites on the orbit can satisfy the communication distance constraint to provide CAV services. Therefore, we have

$$\begin{aligned} P_a^o &= \Pr\left(Q^2 + U^2 \geq \left(\frac{r^2 + r_E^2 - d_{\max}^2}{2r}\right)^2\right) \\ &= \frac{|\omega_1 - \omega_2|}{2\pi} = \frac{\cos^{-1} \left(\frac{\kappa}{\sqrt{\mu^2 + \nu^2}} \right)}{2\pi}. \end{aligned}$$

When there are N satellite orbits, we consider the maximum orbit separation, i.e., adjacent two orbits are separated by π/N for polar orbits and $2\pi/N$ for inclined orbits. Therefore, the probability of having at least one feasible satellite orbit is

$$P_a^o = \begin{cases} \frac{N \cdot |\omega_1 - \omega_2|}{\pi}, & \text{if } \alpha = \frac{\pi}{2} \text{ and } |\omega_1 - \omega_2| \leq \frac{\pi}{N} \\ 1, & \text{if } \alpha = \frac{\pi}{2} \text{ and } |\omega_1 - \omega_2| > \frac{\pi}{N} \\ \frac{N \cdot |\omega_1 - \omega_2|}{2\pi}, & \text{if } \alpha < \frac{\pi}{2} \text{ and } |\omega_1 - \omega_2| \leq \frac{2\pi}{N} \\ 1, & \text{if } \alpha < \frac{\pi}{2} \text{ and } |\omega_1 - \omega_2| > \frac{2\pi}{N}. \end{cases}$$

APPENDIX B PROOF OF PROPOSITION 3

For the first case in (36), T_1 monotonically increases with R . For the second case in (36), we have

$$\begin{aligned} \frac{dT_1}{dR} &= \frac{P_{a,1}}{d_{\max}^2 - h^2} \cdot \frac{d\left(\left(\frac{A_1}{2^{R/B_1} - 1} - h^2\right) \cdot R\right)}{dR} \\ &= \frac{P_{a,1}}{d_{\max}^2 - h^2} \cdot \left[\frac{A_1}{2^{R/B_1} - 1} \left(1 - \frac{R \ln 2}{B_1} \frac{2^{R/B_1}}{(2^{R/B_1} - 1)} \right) - h^2 \right]. \end{aligned}$$

Let $x = R/B_1$ and $f = (R/B_1)[(2^{R/B_1})/(2^{R/B_1} - 1)]$. We have

$$\begin{aligned} f &= \frac{x2^x}{2^x - 1} \\ f' &= \frac{(2^x + x2^x \ln 2)(2^x - 1) - x2^x 2^x \ln 2}{(2^x - 1)^2} \\ &= \frac{2^x}{(2^x - 1)^2} (2^x - 1 - x \ln 2). \end{aligned}$$

Since $(2^x - 1 - x \ln 2)' = 2^x \ln 2 - \ln 2 \geq 0$ when $x \geq 0$, we have $2^x - 1 - x \ln 2$ monotonically increasing with x ($x \geq 0$) and $2^x - 1 - x \ln 2 \geq (2^x - 1 - x \ln 2)_{x=0} = 0$. Therefore, $f' \geq 0$ and f monotonically increases with x ($x \geq 0$). Thus, $f \geq f_{x=0}$. By applying L'hospital's Rule, we have

$$\begin{aligned} \lim_{x \rightarrow 0} \frac{x2^x}{2^x - 1} &= \frac{0}{0} \\ \lim_{x \rightarrow 0} \frac{x2^x}{2^x - 1} &= \lim_{x \rightarrow 0} \frac{(x2^x)'}{(2^x - 1)'} = \lim_{x \rightarrow 0} \frac{2^x + x2^x \ln 2}{2^x \ln 2} = \frac{1}{\ln 2}. \end{aligned}$$

Thus, we have $f \geq (1/\ln 2)$ and

$$\begin{aligned} \frac{dT_1}{dR} &= \frac{P_{a,1}}{d_{\max}^2 - h^2} * \left[\frac{A_1}{2^{R/B_1} - 1} \left(1 - \frac{R \ln 2}{B_1} \frac{2^{R/B_1}}{(2^{R/B_1} - 1)} \right) - h^2 \right] \\ &\leq \frac{P_{a,1}}{d_{\max}^2 - h^2} * \left[\frac{A_1}{2^{R/B_1} - 1} \left(1 - \ln 2 * \frac{1}{\ln 2} \right) - h^2 \right] < 0. \end{aligned}$$

In other words, T_1 in (36) monotonically decreases with R in the second case. Therefore, the maximum throughput is achieved when $R = B_1 \log_2(1 + (A_1/d_{\max}^2))$, which is

$$T_1 = P_{a,1} B_1 \log_2 \left(1 + \frac{A_1}{d_{\max}^2} \right).$$

REFERENCES

- [1] U. Montanaro et al., “Towards connected autonomous driving: Review of use-cases,” *Veh. Syst. Dyn.*, vol. 57, no. 6, pp. 779–814, 2019.
- [2] H. Wang et al., “Architectural design alternatives based on cloud/edge computing for connected vehicles,” *IEEE Commun. Surveys Tuts.*, vol. 22, no. 4, pp. 2349–2377, 4th Quart., 2020.
- [3] J. Chen, H. Wu, P. Yang, F. Lyu, and X. Shen, “Cooperative edge caching with location-based and popular contents for vehicular networks,” *IEEE Trans. Veh. Technol.*, vol. 69, no. 9, pp. 10291–10305, Sep. 2020.
- [4] X. Zhu and C. Jiang, “Creating efficient integrated satellite-terrestrial networks in the 6G era,” *IEEE Wireless Commun.*, vol. 29, no. 4, pp. 154–160, Aug. 2022.
- [5] B. Di, L. Song, Y. Li, and H. V. Poor, “Ultra-dense LEO: Integration of satellite access networks into 5G and beyond,” *IEEE Wireless Commun.*, vol. 26, no. 2, pp. 62–69, Apr. 2019.
- [6] X. Shen et al., “Space-air-ground integrated networks: Review and prospect,” *Chin. J. Internet Things*, vol. 4, no. 3, pp. 3–19, Sep. 2020.
- [7] “Telesat.” Accessed: Feb. 27, 2024. [Online]. Available: <https://www.telesat.com/leo-satellites/>
- [8] “Starlink.” Accessed: Feb. 27, 2024. [Online]. Available: <https://www.starlink.com/>
- [9] “Study on scenarios and requirements for next generation access technologies, Version 17.0.0, (Release 17),” 3GPP, Sophia Antipolis, France, Rep. TR 38.913, Apr. 2022.
- [10] “Service requirements for the 5G system; stage 1, Version 19.0.0, (Release 19),” 3GPP, Sophia Antipolis, France, Rep. TS 22.261, Sep. 2022.
- [11] “Study on new radio (NR) to support non-terrestrial networks, Version 15.4.0, (Release 15),” 3GPP, Sophia Antipolis, France, Rep. TR 38.811, Oct. 2020.
- [12] “Solutions for NR to support non-terrestrial networks (NTN), Version 16.1.0, (Release 16),” 3GPP, Sophia Antipolis, France, Rep. TR 38.821, Jun. 2021.
- [13] “Study on using satellite access in 5G; stage 1, Version 16.0.0, (Release 16),” 3GPP, Sophia Antipolis, France, Rep. TR 22.822, Jul. 2018.
- [14] “Satellite earth stations and systems (SES); combined satellite and terrestrial networks scenarios, document V1.1.1,” ETSI, Sophia Antipolis, France, ETSI TR 103 124, Jul. 2013.
- [15] “Satellite Earth Stations and Systems (SES); overview of present satellite emergency communications resources, V1.2.2,” ETSI, Sophia Antipolis, France, ETSI TR 102 641, Aug. 2013.
- [16] “Satellite earth stations and systems (SES); Multi-link routing scheme in hybrid access network with heterogeneous links, V1.1.1,” ETSI TR 103 351, Jul. 2017.
- [17] D.-H. Jung, J.-G. Ryu, W.-J. Byun, and J. Choi, “Performance analysis of satellite communication system under the shadowed-Rician fading: A stochastic geometry approach,” *IEEE Trans. Commun.*, vol. 70, no. 4, pp. 2707–2721, Apr. 2022.
- [18] K. Guo et al., “Performance analysis of hybrid satellite-terrestrial cooperative networks with relay selection,” *IEEE Trans. Veh. Technol.*, vol. 69, no. 8, pp. 9053–9067, Aug. 2020.
- [19] H. Lin, C. Zhang, Y. Huang, R. Zhao, and L. Yang, “Fine-grained analysis on downlink LEO satellite-terrestrial mmWave relay networks,” *IEEE Wireless Commun. Lett.*, vol. 10, no. 9, pp. 1871–1875, Sep. 2021.
- [20] J. Ye, G. Pan, and M.-S. Alouini, “Earth rotation-aware non-stationary satellite communication systems: Modeling and analysis,” *IEEE Trans. Wireless Commun.*, vol. 20, no. 9, pp. 5942–5956, Sep. 2021.
- [21] P. K. Sharma, B. Yogesh, D. Gupta, and D. I. Kim, “Performance analysis of IoT-based overlay satellite-terrestrial networks under interference,” *IEEE Trans. Cogn. Commun. Netw.*, vol. 7, no. 3, pp. 985–1001, Sep. 2021.
- [22] A. Guidotti et al., “Architectures and key technical challenges for 5G systems incorporating satellites,” *IEEE Trans. Veh. Technol.*, vol. 68, no. 3, pp. 2624–2639, Mar. 2019.
- [23] S. Kota, G. Giambene, and S. Kim, “Satellite component of NGN: Integrated and hybrid networks,” *Int. J. Satell. Commun. Netw.*, vol. 29, no. 3, pp. 191–208, Apr. 2011.
- [24] N. Zhang, S. Zhang, P. Yang, O. Alhussain, W. Zhuang, and X. Shen, “Software defined space-air-ground integrated vehicular networks: Challenges and solutions,” *IEEE Commun. Mag.*, vol. 55, no. 7, pp. 101–109, Jul. 2017.
- [25] H. Wu et al., “Resource management in space-air-ground integrated vehicular networks: SDN control and AI algorithm design,” *IEEE Wireless Commun.*, vol. 27, no. 6, pp. 52–60, Dec. 2020.
- [26] Z. Niu, X. Shen, Q. Zhang, and Y. Tang, “Space-air-ground integrated vehicular network for connected and automated vehicles: Challenges and solutions,” *Intell. Conver. Netw.*, vol. 1, no. 2, pp. 142–169, Sep. 2020.
- [27] T.-X. Zheng et al., “Physical-layer security of uplink mmWave transmissions in cellular V2X networks,” *IEEE Trans. Wireless Commun.*, vol. 21, no. 11, pp. 9818–9833, Nov. 2022.
- [28] I. Leyva-Mayorga et al., “NGSO constellation design for global connectivity,” 2022, *arXiv:2203.16597*.
- [29] “Base station (BS) radio transmission and reception, Version 17.7.0, (Release 17),” 3GPP, Sophia Antipolis, France, Rep. TS 38.104, Sep. 2022.



Huaqing Wu (Member, IEEE) received the B.E. and M.E. degrees from Beijing University of Posts and Telecommunications, Beijing, China, in 2014 and 2017, respectively, and the Ph.D. degree from the University of Waterloo, Waterloo, ON, Canada, in 2021.

She is currently an Assistant Professor with the Department of Electrical and Software Engineering, University of Calgary, Calgary, AB, Canada. Her current research interests include B5G/6G, space-air-ground integrated networks, Internet of

vehicles, mobile/edge computing/caching, and artificial intelligence for future networking.

Dr. Wu received Best Paper Awards at IEEE GLOBECOM 2018, *Chinese Journal on Internet of Things* 2020, and IEEE GLOBECOM 2022. She has been serving as an Associate Editor of IEEE NETWORK since 2023 and *Security and Safety* since 2021.



Mingcheng He (Graduate Student Member, IEEE) received the B.S. and M.Eng. degrees from Shanghai Jiao Tong University, Shanghai, China, in 2017 and 2020, respectively. He is currently pursuing the Ph.D. degree with the Department of Electrical and Computer Engineering, University of Waterloo, Waterloo, ON, Canada.

His research interests include network slicing in satellite-terrestrial integration networks and machine learning in future wireless networks.



Xuemin (Sherman) Shen (Fellow, IEEE) received the Ph.D. degree in electrical engineering from Rutgers University, New Brunswick, NJ, USA, in 1990.

He is a University Professor with the Department of Electrical and Computer Engineering, University of Waterloo, Waterloo, ON, Canada. His research focuses on network resource management, wireless network security, Internet of Things, 5G and beyond, and vehicular networks.

Dr. Shen received the “West Lake Friendship Award” from Zhejiang Province in 2023, the President’s Excellence in Research from the University of Waterloo in 2022, the Canadian Award for Telecommunications Research from the Canadian Society of Information Theory in 2021, the R.A. Fessenden Award in 2019 from IEEE, Canada, the Award of Merit from the Federation of Chinese Canadian Professionals (Ontario) in 2019, the James Evans Avant Garde Award in 2018 from the IEEE Vehicular Technology Society, the Joseph LoCicero Award in 2015 and the Education Award in 2017 from the IEEE Communications Society (ComSoc), and the Technical Recognition Award from Wireless Communications Technical Committee in 2019 and AHSN Technical Committee in 2013. He has also received the Excellent Graduate Supervision Award from the University of Waterloo in 2006 and the Premier’s Research Excellence Award from the Province of Ontario, Canada, in 2003. He served as the Editor-in-Chief of the IEEE INTERNET OF THINGS JOURNAL, IEEE NETWORK, and *Peer-to-Peer Networking and Applications*. He serves/served as the General Chair for the 6G Global Conference’23 and ACM Mobihoc’15, the Technical Program Committee Chair/Co-Chair for IEEE Globecom’24, 16, and 07, IEEE Infocom’14, and IEEE VTC’10 Fall, and the Chair for the IEEE ComSoc Technical Committee on Wireless Communications. He is a registered Professional Engineer of Ontario, Canada, an Engineering Institute of Canada Fellow, a Canadian Academy of Engineering Fellow, a Royal Society of Canada Fellow, a Chinese Academy of Engineering Foreign Member, and a Distinguished Lecturer of the IEEE Vehicular Technology Society and Communications Society. He was the President of the IEEE ComSoc, the Vice President for Technical and Educational Activities, the Vice President for Publications, a Member-at-Large on the Board of Governors, the Chair of the Distinguished Lecturer Selection Committee, and a member of IEEE Fellow Selection Committee of the ComSoc.



Weihua Zhuang (Fellow, IEEE) received the B.Sc. and M.Sc. degrees in electrical engineering from Dalian Maritime University, Dalian, China, in 1982 and 1985, respectively, and the Ph.D. degree in electrical engineering from the University of New Brunswick, Fredericton, NB, Canada, in 1993.

She is a University Professor and a Tier I Canada Research Chair of Wireless Communication Networks with the University of Waterloo, Waterloo, ON, Canada. Her research focuses on network architecture, algorithms and protocols, and service

provisioning in future communication systems.

Dr. Zhuang is a recipient of the 2021 Women's Distinguished Career Award from IEEE Vehicular Technology Society, the 2021 Technical Contribution Award in Cognitive Networks from IEEE Communications Society, the 2021 R. A. Fessenden Award from IEEE Canada, and the 2021 Award of Merit from the Federation of Chinese Canadian Professionals in Ontario. She was the Editor-in-Chief of the IEEE TRANSACTIONS ON VEHICULAR TECHNOLOGY from 2007 to 2013, the General Co-Chair of 2021 IEEE/CIC International Conference on Communications in China, the Technical Program Chair/Co-Chair of IEEE VTC2017/2016-Fall, the Technical Program Symposia Chair of 2011 IEEE Globecom, and an IEEE Communications Society Distinguished Lecturer from 2008 to 2011. She is an elected member of the Board of Governors and the President of the IEEE Vehicular Technology Society. She is a Fellow of the Royal Society of Canada, Canadian Academy of Engineering, and Engineering Institute of Canada.



Ngọc-Dũng Đào received B.Eng. degree in communications engineering from the Hanoi University of Science and Technology, Hanoi, Vietnam, in 1995, the M.Eng. degree in telecommunications from the Asian Institute of Technology, Bangkok, Thailand, in 2002, and the Ph.D. degree in electrical and computer engineering from the University of Alberta, Edmonton, Canada, in 2007.

From 2007 to 2010, he was with Toshiba Research Europe, Bristol, U.K., Since 2010, he has been with Huawei Technologies Canada. He is a Principle

Engineer with Huawei Technologies Canada, Inc., Ottawa, ON, Canada. His recent research interests include 6G mobile network architectures, data analytics, vehicle communications, IoT, digital twin, and metaverse.

Dr. Đào has served on the editorial boards of IEEE COMMUNICATIONS SURVEY AND TUTORIALS, IEEE TRANSACTIONS ON VEHICULAR TECHNOLOGY, IEEE COMMUNICATIONS LETTERS, and *IEEE Communications Magazine*.



Weisen Shi (Member, IEEE) received the B.S. degree from Tianjin University, Tianjin, China, in 2013, the M.S. degree from Beijing University of Posts and Telecommunications, Beijing, China, in 2016, and the Ph.D. degree from the Department of Electrical and Computer Engineering, University of Waterloo, Waterloo, ON, Canada, in 2020.

He is currently a Senior Engineer with Huawei Technologies Canada, Inc., Ottawa, ON, Canada. His interests include AI in networks, space-air-ground integrated networks, UAV communication and networking, and RAN slicing.